



Microstructural and Mechanical Behavior of Al6061-Graphene Oxide Nanocomposites

Mahdi Hedayatian¹ · Khodadad Vahedi¹ · Alireza Nezamabadi¹ · Amir Momeni²

Received: 27 February 2019 / Accepted: 4 July 2019 / Published online: 24 July 2019
© The Korean Institute of Metals and Materials 2019

Abstract

In this paper, the mechanical properties and microstructure of Al6061-graphene oxide (GO) nanocomposites material, produced by stir casting and hot rolling process have been investigated. In order to make composite samples, GO nanoplates with various weight percents of 0.2, 0.5 and 0.8% were added to the molten Al6061 through the stir casting process. Then the cast composite slabs were hot rolled at 530 °C. Tensile and hardness tests were used to study the mechanical properties of nanocomposite specimens. The microstructures of samples were examined by optical and scanning electron microscopes. The scanning electron microscope images and energy dispersive spectroscopy map analyses showed that the GO nanoplates have been uniformly distributed within the Al matrix. The mechanical test results showed considerable improvements in the hardness (by 41%), yield strength (by 43%), tensile strength (by 38%), ductility (by 58%) and toughness (by 116%) of the composite samples with respect to the base alloy. Studying the fracture surface also showed that ductile fracture is the dominant mechanism of fracture in all the specimens.

Keywords Metal matrix composite · Nanocomposite · Stir casting · Graphene oxide · Al6061

1 Introduction

Particulate reinforced metal matrix composites (MMCs) have the potential to provide tailored mechanical properties, for example, high specific stiffness and specific strength and creep resistance, which render them attractive for several industrial applications [1, 2].

In the recent years, aluminum matrix composites (AMCs) have been widely used in aerospace, military and automotive industries owing to their low densities, excellent mechanical properties, and low production costs [3–5]. So far, the effect of many reinforcing particles, such as Al₂O₃ [6, 7], SiC [8, 9], TiB₂ [10, 11] and B₄C [12, 13] on the aluminum matrix has been investigated. The addition of reinforcing particles in micron size usually degrades the ductility of composites. This weakness has encouraged researchers to use nanoparticles instead of micro particles in MMCs [14].

Carbon allotropes and its nanostructures such as carbon nanotube (CNT), fullerene, nanofiber, and graphene are promising reinforcement materials for aluminum matrix nanocomposites (AMNCs) owing to their unique thermal, electrical, mechanical, and tribological properties [15]. Recently, Graphene oxide has also attracted a great deal of attention due to its unique structure and outstanding properties [16]. In 2004, a new structure of carbon, called graphene, was produced with some superior properties than carbon nanotubes. It is a nano sizedplate like material with Young modulus of 1 TPa and tensile strength of 130 GPa [17]. Such unique properties have introduced graphene and graphene oxide (GO) as good reinforcing materials for aluminum matrices. Having lower density than aluminum, graphene and GO not only lower the weight of composite components, but also ameliorate their mechanical properties [18]. The presence of oxygen functional groups (hydroxyl, carboxyl, carbonyl and epoxy) in GO enable it to well interact with the metallic matrix materials and make strong bonding [19].

Different solid, gas and liquid state methods have been so far used to produce AMCs [1]. Amongst the methods, compocasting and subsequent metal forming processes have been the major processing route for fabricating bulk AMCs [20].

✉ Alireza Nezamabadi
a-nezamabadi@iau-arak.ac.ir

¹ Department of Mechanical Engineering, Arak Branch, Islamic Azad University, Arak, Iran

² Department of Materials Science and Engineering, Hamedan University of Technology, Hamedan, Iran

Generally, the metal forming processes increase the mechanical properties by removing inhomogeneities and porosities and uniform dispersing the particles within the matrix [21–26].

Despite the valuable works on the fabrication and properties of AMCs in the cited literature, less attention has been paid to the AMCs with GO. The mechanical properties of Al-GO composites have been the hot spot in these researches. It has been reported that the addition of graphene or GO increase strength in the expense of ductility [27–30]. In most of the works AMCs have been fabricated in small scales using powder metallurgy and mechanical milling or surface coating by friction stir processing (FSP) and less attention has been paid to bulk AMCs. Therefore, the microstructure and mechanical properties of bulk AMCs with graphene and graphene oxide still need further investigations.

The present study was defined in this context and aimed to contribute to a better understanding of microstructure and mechanical properties of bulk Al6061-GO nanocomposites. In this research, the bulk nanocomposites were fabricated by compocasting and hot rolling processes and then examined by mechanical testing and microstructural observations.

2 Materials and Methods

2.1 Materials

In this study Al6061 aluminum alloy with chemical composition given in Table 1 (according to the ASTM-E1259 standard) and graphene oxide (GO: US research Nanomaterials company) were used as the matrix and reinforcing particles, respectively. The physical properties of the graphene oxide nanoplates are given in Table 2.

2.2 Fabrication of Composites

Graphene oxide is commonly synthesized using the modified Hammers' method [31, 32]. Typically, 4 g natural graphite (1–8 μm), 4 g NaNO_3 , and 184 mL H_2SO_4 are mixed together in an ice bath, while 12 g KMnO_4 is added slowly to the suspension under stirring. The adding process is extremely slow to prevent the temperature from exceeding 20 $^\circ\text{C}$. After reaction for 2 h, the mixed suspension is heat-treated at 35 $^\circ\text{C}$ by using oil bath and maintained for 1 h. Approximately 184 mL of H_2O is slowly poured into the above suspension. Then the suspension is thermally treated at 98 $^\circ\text{C}$ for 40 min. The suspension is treated by 30% H_2O_2 solution ultimately. The final product is washed with 4% dilute HCl solution, collected and dried. Then the GO nanoplates were initially dispersed into

Table 2 Physical properties of the GO nanoplates

Parameter	Value
Thickness	3.4–7 (nm)
Number of layers	6–10
Diameter	1–8 (micron)
Density	1 (gr/cm^3)
Specific surface area	750 (m^2/g)
Volume resistivity	4×10^{-4} ($\Omega \text{ cm}$)

acetone and sonicated for 10 min using ultrasonic probes to separate the agglomerated particles (Fig. 1a). The emulsion was then sprayed on an aluminum foil and let acetone evaporate from the surface (Fig. 1b). The foils were then encapsulated to be readily added to the molten Al.

Then, the small pieces of aluminum Al6061 (1.5 kg), were melted by heating up to 700 $^\circ\text{C}$. About 1 wt% magnesium was added to the melt to enhance the wettability of GO particles with the aluminum matrix [33]. After melt degassing by Hexachloroethane (C_2Cl_6) tablets the surface of melt was coated with a flux coverall in order to prevent the oxygen absorption. The GO capsules were preheated to 600 $^\circ\text{C}$ for 30 min and then added to the molten Al6061 to produce composites with 0.2, 0.5 and 0.8 wt% of GO. These values correspond to 0.54, 1.34 and 2.13 vol% of GO in Al. Volume percent in composites can be related to the weight percent as follows:

$$V_f = w_t (w_t + (1 - w_t) \rho_f / \rho_m)^{-1} \quad (1)$$

where ρ_f and ρ_m are the densities of graphene oxide and Al6061 matrix, respectively. The composite melts were then stirred for 10 min at a constant stirring rate of 400 rpm. The resulting melt was then injected into a pre-heated two-piece cube-shaped steel mold in dimensions of 100 \times 150 \times 33 mm. For comparison, a sample of the base alloy was stirred with the same procedure of preparing composites, but without any addition of GO.

In order to homogenize the chemical composition and remove segregations, the casting ingots were heated up to 580 $^\circ\text{C}$ in an electric furnace and held for 2 h and then rapidly cooled to the ambient temperature. In order to remove all imperfections, such as porosity resulting from stir casting operations, as well as heterogeneous chemical composition, castings ingots were subjected to hot rolling. After reheating at 530 $^\circ\text{C}$, cast ingots were hot rolled by 8 passes to reduce the thickness from 33 to 4.2 mm. The thickness reduction was

Table 1 Chemical composition of Al6061 alloy (wt%)

Al	Mg	Si	Fe	Cu	Cr	Ti	Mn	Zn	Ni
Rem.	0.79	0.51	0.39	0.19	0.09	0.04	0.01	0.01	0.005

Fig. 1 Preparation steps of GO powder: **a** sonication of GO in acetone with an ultrasonic probe, **b** mixture sprayed on aluminum foil

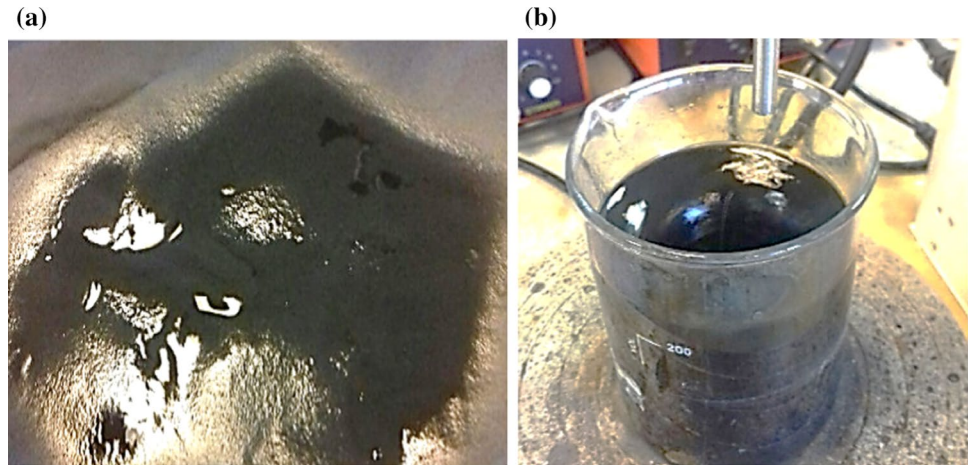
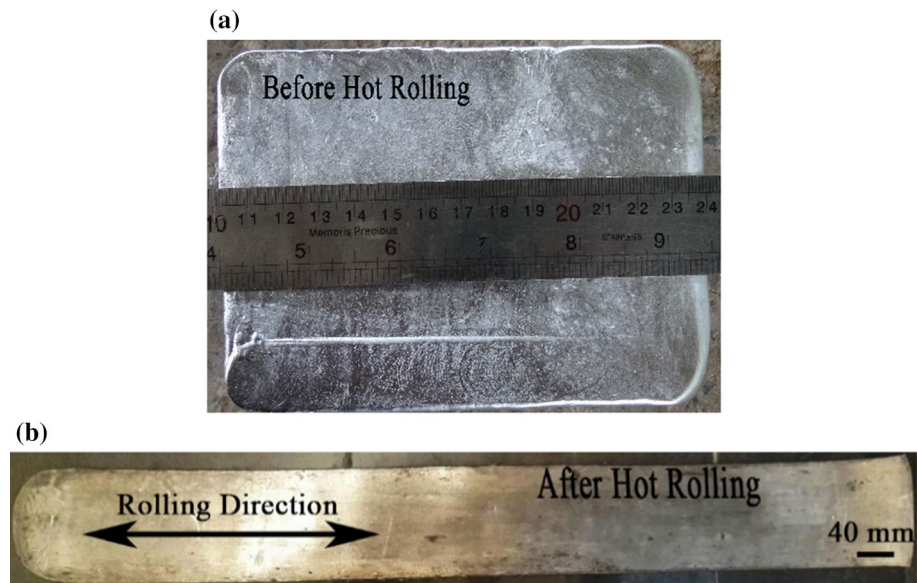


Fig. 2 Representative images of **a** cast and **b** rolled Al6061-0.5 wt% GO sample



about 80% during the 8 passes of hot rolling process. Figure 2 shows images of the cast and rolled samples.

2.3 Mechanical Testing

To determine the tensile strength of Al6061-GO composites some dog-bone specimens were cut off from the rolled plates parallel to the rolling direction and machined according to the ASTM-B 557 standard (Fig. 3). The tensile tests were carried out by SANTAM STM-150 universal testing machine at constant cross-head speed of 1 mm/min. For each composite (each weight percentage of GO), three samples were tested to ensure reproducibility of the stress–strain results. The hardness samples were polished with sand paper of mesh 400 and then subjected to the Vickers indenter at load of 30 kgf for 15 s according to the standard ASTM-E92. The hardness values were determined from the average of 5 hits.

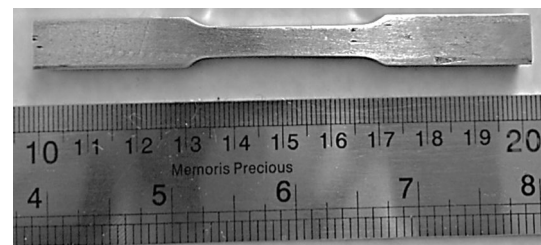


Fig. 3 A representative image of tensile test sample (Al6061-0.2 wt% GO)

In order to evaluate the amount of porosity in the samples, the actual densities were firstly measured by using the Archimedes method according to ISO2738 standard. The porosity values were determined from the average of 5 samples in each weight percentage of GO. Eventually, data scatter information (error bar and \pm range based on the testing of

multiple specimens of each type) were reported by evaluating the standard deviation.

2.4 Microstructural Investigations

For microstructural observations, the samples were prepared by the standard metallographic techniques and chemically etched in ferric chloride solution (2 ml HF, 3 ml HCl, 5 ml HNO₃ and 190 ml H₂O) for 30 s. The microstructure and fracture surface of tensile samples were investigated by optical microscopy (OM, union) and scanning electron microscopy (SEM, JEOL).

3 Results and Discussion

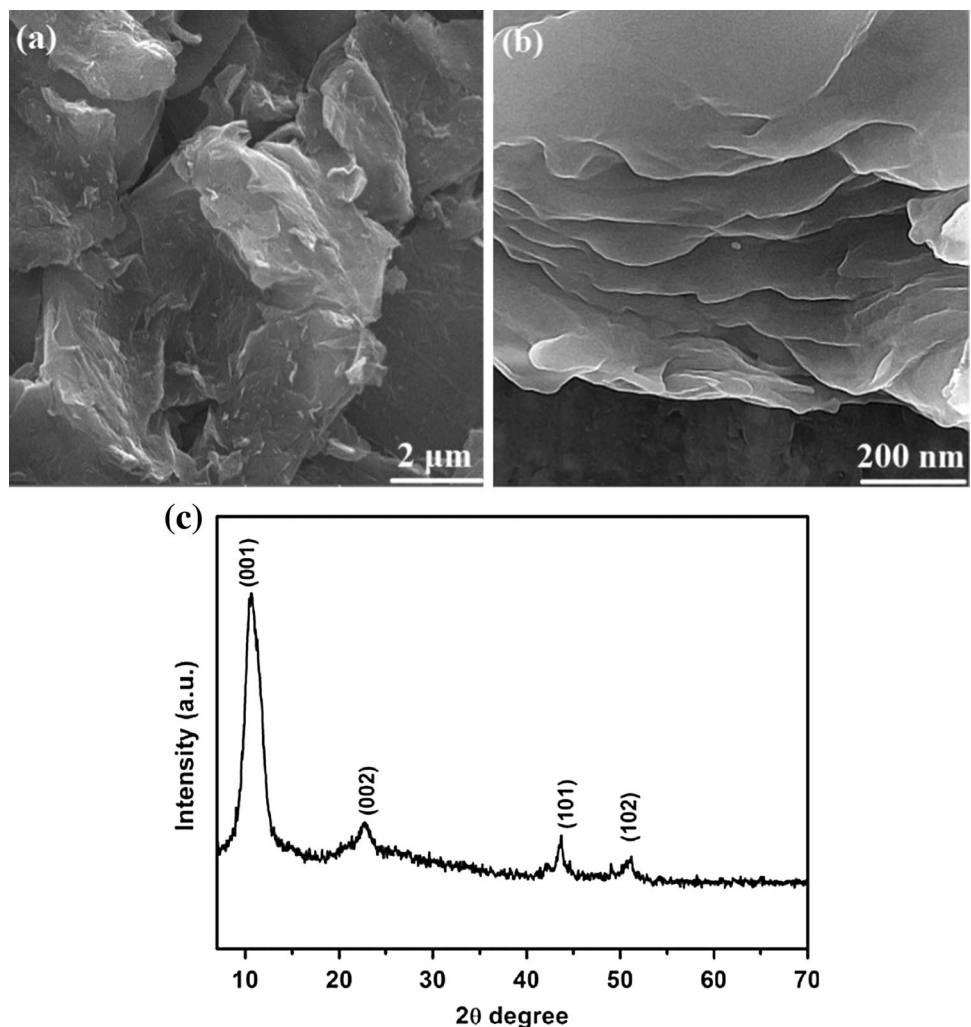
3.1 Microstructural Observations

Figure 4 shows the FESEM micrographs and X-ray diffraction (XRD) spectrum from the GO powder remained after

the evaporation of acetone on the Al foils. In the FESEM images, Fig. 4a, b, the sheet-like structure of GO is revealed and the size of reinforcements is confirmed in the range specified by the supplier (1–8 microns). It should be noted that according to Table 2, the GO particles are actually in shape of plates with nano-sized thickness, but other dimensions are in micrometer scale. This feature imparts them high specific surface area, which is 12.8 times larger than that of carbon nanotubes [30]. Hence, in the literature, they are often referred to as “nanosheets” or “nanoplates”.

The Van der Waals attracting force is responsible for the attachment of nanoplates to each other. It is expected that the force stirring paddle to come over the Van der Waals attracting force and help the nanoplates to uniformly distribute within the molten Al6061. The XRD spectrum is shown in Fig. 4c clearly indicates the major peak of GO at $2\theta = 11.5^\circ$, which is corresponding to the strong diffraction from (002) planes [34]. The absence of a peak at $2\theta = 25^\circ\text{--}30^\circ$ indicates that the original graphene has been completely converted into GO and other impurities like graphite are absent. It

Fig. 4 a, b FESEM micrographs from the GO nanoplates used in this investigation with two different magnifications, c XRD spectrum of the GO powder



is therefore confirmed that the reinforcing particle is high purity GO.

The interlayer spacing of the GO samples can be calculated by the Bragg's law:

$$2d\sin\theta = n\lambda \quad (2)$$

where d is the interlayer spacing, θ is the diffraction angle of characteristic peak and λ is the wavelength of the X-ray beam (0.154 nm for Cu tube) and n is a positive integer (equal to unity in this study) [35]. As seen in Fig. 4c, the diffraction peak position is at $2\theta = 11.5^\circ$, representing the (001) planes, the spacing between the GO layers can be calculated as follows:

$$d = \frac{n\lambda}{2\sin\theta} = \frac{1 \times 0.154}{2 \times \sin(5.8^\circ)} = 0.762 \text{ nm} \quad (3)$$

It indicated that the spacing between sheets was 0.762 nm, which was caused by the oxygenated groups in between the sheets. The calculated interlayer spacing is in good agreement with 0.865 nm [36] and 0.790 nm [32], respectively.

Figure 5 shows the optical micrographs of the hot rolled samples. The decreasing trend in the average grain size of Al matrix with increase in the amount of GO is evident in the micrographs. By using ImageJ analyzer software the average grain size of the pure sample (Fig. 5a) and the composites with 0.2, 0.5 and 0.8 wt% GO was measured as 350, 257, 182 and 108 microns, respectively.

As schematically shown in Fig. 6, the role of GO nanoplates in the observed grain refinement in three steps can be separated as follows: (a, b)-the refinement of cast

microstructure by acting as the nucleant and (c, d)-the refinement of hot rolled microstructure by inhibiting excessive grain growth. During the solidification stage of composites GO particles can act as nucleants. This effectively helps the nucleation step and increases the rate of solidification. In composites of Al7068 containing graphene nanoplates the change in the morphology of grains from coarse columnar grains to fine equiaxed ones has been reported [37]. The solidification regime changes in the composites and the nuclei formed on the nanoplates everywhere in the molten Al act as barriers against the excessive directional growth of other nuclei.

According to the literature, graphite and graphene have limited wettability with liquid Al [38, 39]. Even though the wettability is increased by adding Mg to molten Al, the contact angle (θ) barely falls below 130° . Despite this low wettability, it can be proved that GO particles increase the rate of solidification and refine the cast microstructure. The nucleation rate (\dot{N}) can be related to the energy barrier for nucleation (ΔG^*) by using the following equation [40]:

$$\dot{N} = C \cdot \exp\left(-\frac{\Delta G^*}{kT}\right) \quad (4)$$

where C is a constant dependent on the rate of atomic diffusion from the solid/liquid interface, k is the Boltzman constant and T is the absolute solidification temperature. On the basis of Eq. (4), the nucleation rates with and without the contribution of GO particles as nucleants (\dot{N} and \dot{N}_{GO}) can be compared using the following equation:

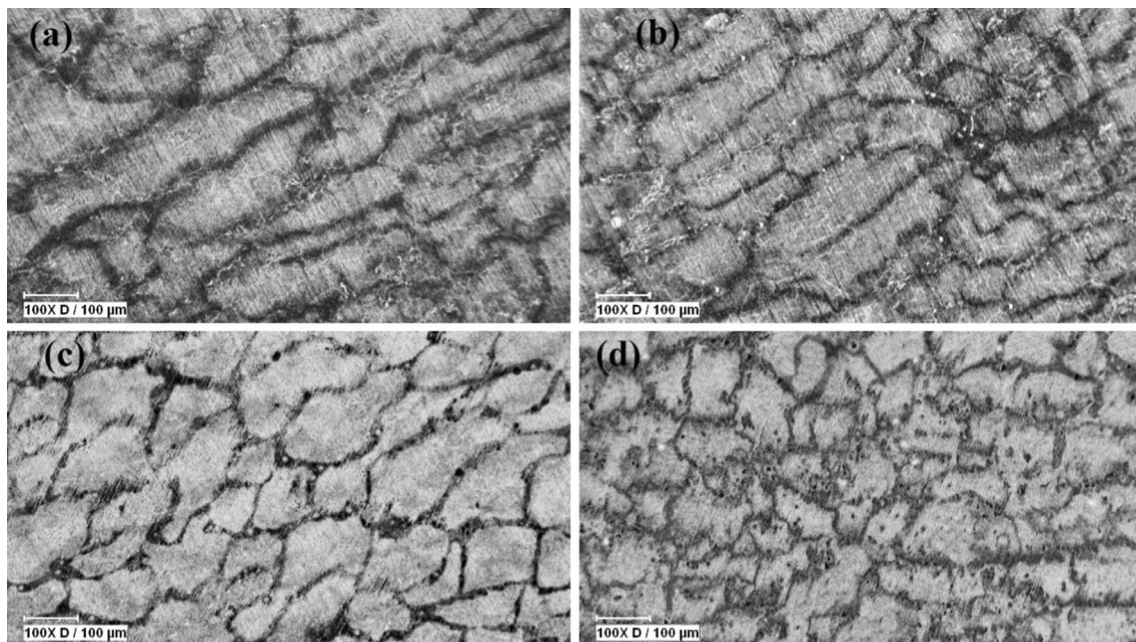


Fig. 5 Optical micrographs of hot rolled samples: **a** pure Al6061, **b** Al6061-0.2 wt% GO, **c** Al6061-0.5 wt% GO, **d** Al6061-0.8 wt% GO

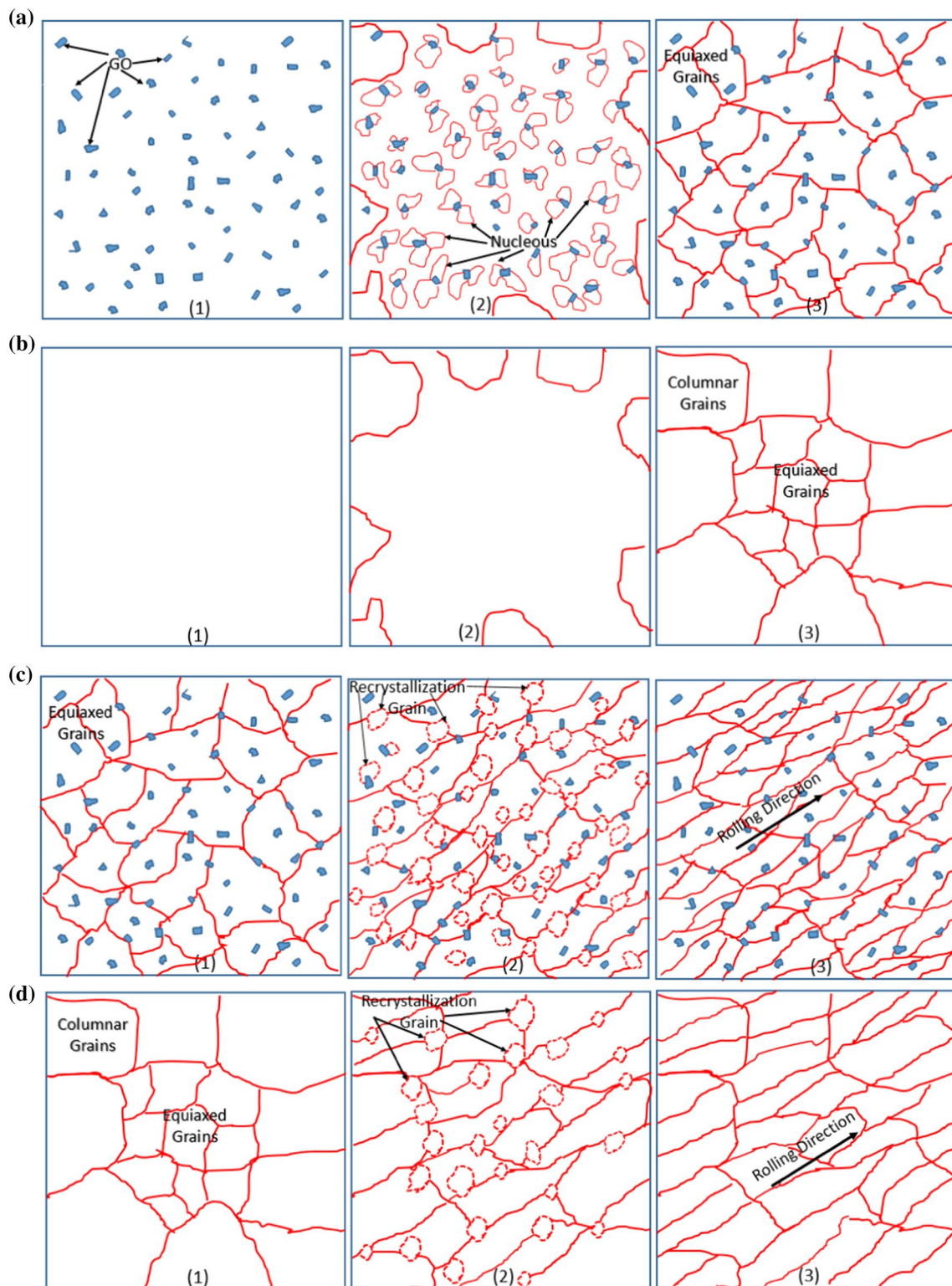


Fig. 6 Schematic representation of grain refinement: **a** solidification process in the composites, showing GO particles work as the preferential nucleation sites, **b** solidification process in the alloy without

GO, **c** recrystallization process in the hot rolled composites, **d** recrystallization process in the hot rolled pure alloy without GO in three steps (left to right)

$$\frac{\dot{N}_{GO}}{\dot{N}} \approx \exp\left(\frac{\Delta G^* - \Delta G_{GO}^*}{kT}\right) \quad (5)$$

Here ΔG_{GO}^* is the activation energy for the nucleation of Al nuclei on the surface of GO nanoplates. In general, there is a simple relationship between ΔG^* (homogeneous spherical nucleation) and ΔG_{GO}^* (heterogeneous cap-shaped nucleation) as follows [41]:

$$\Delta G_{GO}^* = \Delta G^* \cdot s(\theta) \quad (6)$$

where $s(\theta)$ is a shape factor depending on the wetting angle as $(2 + \cos\theta)(1 - \cos\theta)^2/4$. Combining Eqs. (5) and (6) yields:

$$\frac{\dot{N}_{GO}}{\dot{N}} \approx \exp((1 - s(\theta))G_0) \quad (7)$$

Taking $\theta = 130^\circ$ and $s(\theta) = 0.9$ and $G_0 \approx 78$ [41], it is concluded that the rate of solidification in presence of GO particles can be very higher than that of the original condition. It is also clear that \dot{N}_{GO}/\dot{N} increases with increase in the amount of GO, if the particles are well dispersed within the molten alloy.

The second role of GO particles in the microstructure of composites is to hinder the grain growth during hot rolling. During the hot rolling process the cast structure turns into a wrought one through the recrystallization and growth of new equiaxed grains [42, 43]. In the composites, the GO particles

inhibit the excessive growth of the recrystallized grains giving rise to a fine-grained microstructure. The radius (r) and volume fraction (f_v) of particles are two major factors which control the recrystallized grain size. The equation, called the Zener equation, defines the grain size surrounded by the particles (d_z) as follows:

$$d_z = \frac{4\alpha r}{3f_v} \quad (8)$$

where α is a constant in the order of unity. Based on this equation, the grain size in the hot rolled composites should decrease with increase in the volume fraction of GO nanoplates. However, when the agglomeration of the particles takes place, r increases and the effects of r and f_v are balanced and d_z remains constant.

SEM micrographs of the composites showing the distribution of GO particles are exhibited in Fig. 7. The white arrows point to the porosities formed adjacent to the GO particles and the red arrows show the GO particles. The lower amount of dark spots in the base alloy suggests that the air confined between GO particles should be the major reason for the porosity formation in the composites. It appears that at 0.2 wt% GO composite, Fig. 7b, fine GO particles with the average diameters of 1–8 microns have been well dispersed in the matrix. However, with increase in the GO content to 0.5 and 0.8 wt%, Fig. 7c, d, larger particles appeared due to the particle agglomeration. This, in turn, indicates that

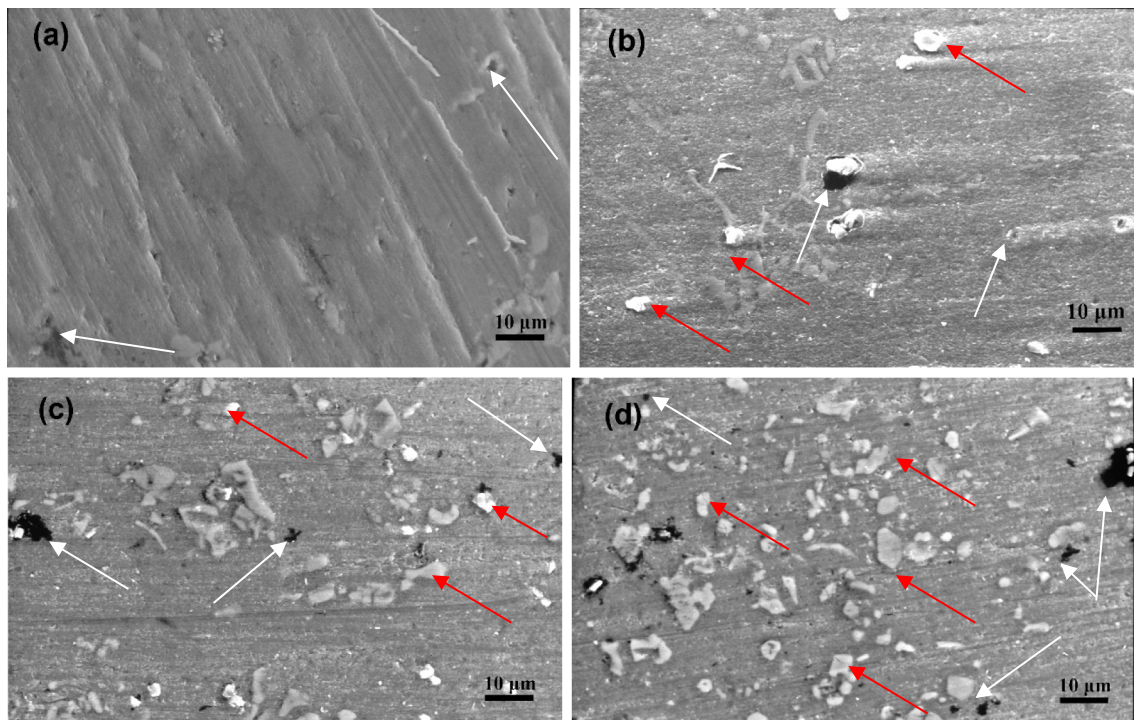
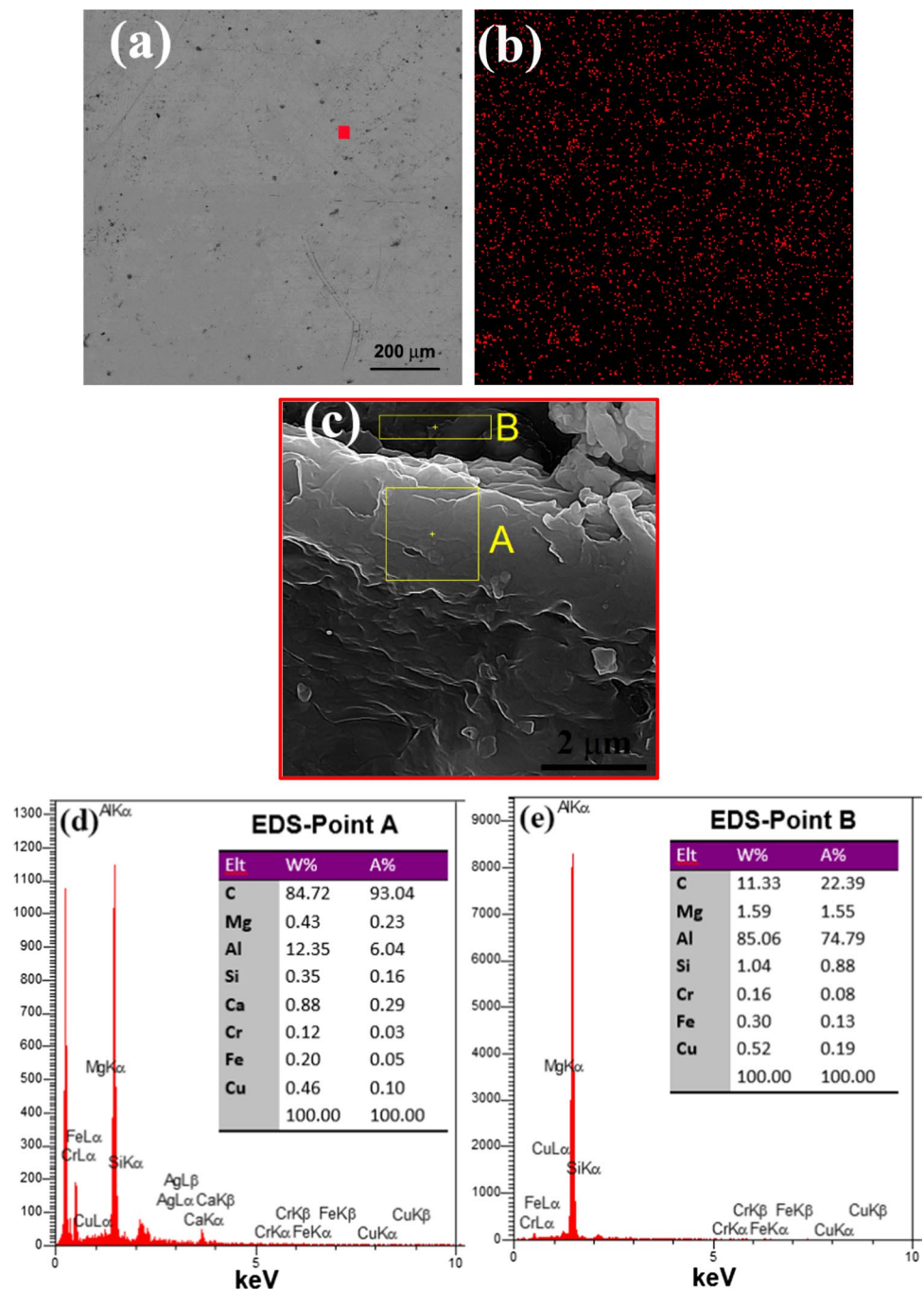


Fig. 7 SEM micrographs of the fabricated samples: **a** base Al6061, **b** Al6061-0.2 wt% Go, **c** Al6061-0.5 wt% GO, **d** Al6061-0.8 wt% GO

Fig. 8 **a** FESEM view of the Al6061-0.8 wt% Go sample, **b** EDS map of C-K α showing the uniform distribution of GO particles within the Al matrix, **c** magnified view of the point colored red in **a**. **d**, **e** local EDS from points denoted as A and B in **c**. (Color figure online)



in composite with 0.2 wt% GO the stirring force is enough to break the primary attracting force between particles. However, in composite containing 0.5 wt% GO and more in 0.8 wt% GO, shorter distance between the particles in the melt helps them to reaggregate after detaching by the stirring force. Although it is clear that in a composite with higher amount of nanoplates the possibility for the adherence of particles by the attracting Van der Waals forces increases, some processing parameters like the temperature gradient during solidification and the concentration gradient

of alloying elements in the freezing front may be also effective [44].

Figure 8 exhibits some quantitative analysis carried out by FESEM on the composite alloy with 0.8 wt% GO. The backscattered image and EDS map of carbon in Fig. 8a, b indicate that the GO particles have been nearly uniformly distributed within the Al matrix. The focused view of specified location in Fig. 8c and local EDS analysis from the points A and B in Fig. 8d, e signifies the coexistence of GO and Al matrix, respectively.

The porosity percentage in the samples before and after the hot rolling process was calculated according to the difference between the theoretical and measured density by the Archimedes method (described in Sect. 2.4). The results of measurement in Fig. 9 show that the sample without GO contains only about 0.67 vol% porosity. This means that a minor part of porosity should be ascribed to the stirring action. On average, after performing the hot rolling process, the porosity decreased by about 56% compared to the casting state. It is also evident that the amount of porosity increases with increase in the amount of GO. The micrographs of Fig. 7 show that the microporosities are mainly observed around the GO particles. The inhomogeneous deformation around the large GO particles helps such porosities to survive during hot rolling.

3.2 Mechanical Properties

In Fig. 10, the image of the broken specimen and the necking surface in the fracture area shows a ductile fracture, and the engineering stress–strain curves of the samples fabricated by stir casting and hot rolling are shown in Fig. 11. It is observed that both the strength and ductility of samples have been considerably ameliorated with increase in the amount of GO.

The values of yield strength (0.2% proof stress method), ultimate tensile strength, total elongation and fracture

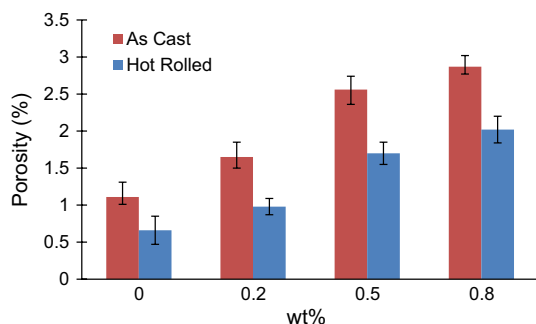
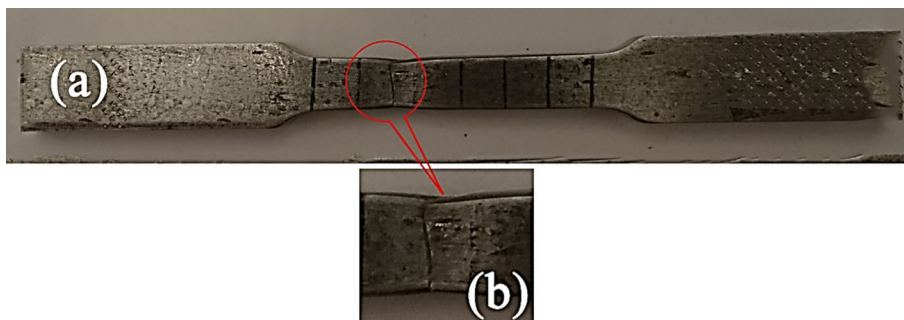


Fig. 9 Volume percent of microporosity in the fabricated samples before and after the hot rolling process

Fig. 10 **a** Broken tensile samples of Al6061-0.2%GO, **b** enlarged picture of necking area



toughness energy (the area below the stress–strain curves) were determined using the standard methods and summarized in Table 3. The quantities clearly indicate that the highest strength, ductility and toughness are obtained in the sample with 0.8 wt% GO. The increase in the yield strength (S_y), tensile strength (S_{uts}), ductility (elongation %) and toughness (T), in the sample containing 0.8 wt% GO with respect to the pure aluminum alloy sample were about 43, 38, 58 and 116%, respectively.

Figure 12 shows the percent of improvement in the mechanical properties of fabricated composites with respect to the pure Al6061 as functions of GO content. It is worthy to note that, S_y , S_{uts} , toughness and elongation show increasing trend with the GO content.

The strengthening increment of reinforcement on the Al matrix (R), can be based on the below equation:

$$R = 100 \times (\sigma_c - \sigma_m) / \sigma_m \quad (9)$$

where σ_c and σ_m are the UTS of the composite and matrix, respectively. Figure 13, indicates that the here improvements in the mechanical properties are much more better than other published reports [27, 28, 45–48]. As a conclusion, GO can play a role of desirable filler material in Al nanocomposites. The strengthening capacity of GO in the nanocomposites can be better recognized by comparing its strengthening and

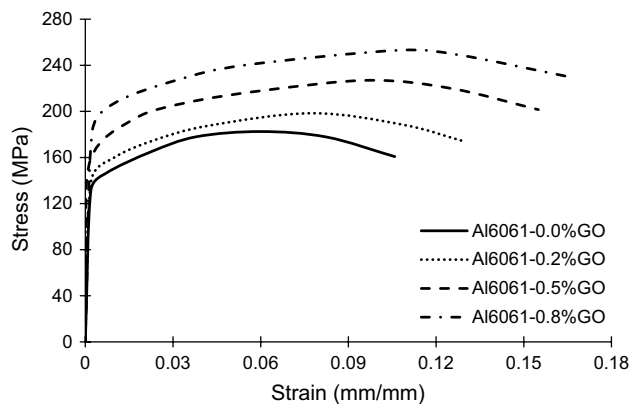


Fig. 11 Engineering stress–strain curves of the fabricated samples

Table 3 Quantities of the yield and ultimate tensile strengths (S_y and S_{uts}), elongation ($\delta\%$) and toughness (T) for the fabricated samples

Sample	wt%	V_f %	S_y (MPa)	S_{uts} (MPa)	δ (%)	T (MJ m ⁻³)
Al6061-0.0%GO	0.0	0.0	129 ± 6	182 ± 9	10.6 ± 0.1	17.9 ± 0.3
Al6061-0.2%GO	0.2	0.54	140 ± 5	198 ± 7	13.0 ± 0.3	23.6 ± 0.3
Al6061-0.5%GO	0.5	1.34	159 ± 9	227 ± 11	15.6 ± 0.1	27.9 ± 0.2
Al6061-0.8%GO	0.8	2.13	185 ± 8	251 ± 7	16.7 ± 0.2	38.6 ± 0.5

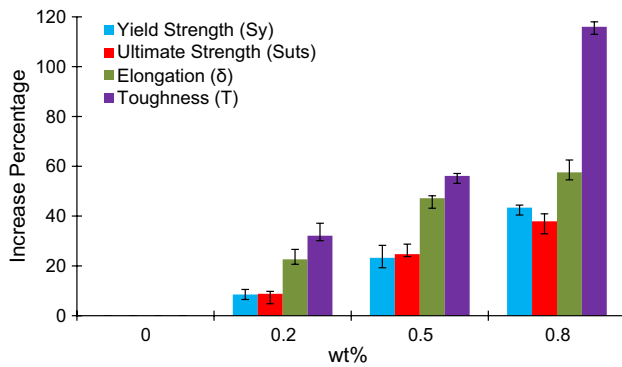


Fig. 12 Percentage of improvement in the mechanical properties of fabricated composites with respect to the pure Al6061 alloy as functions of GO content

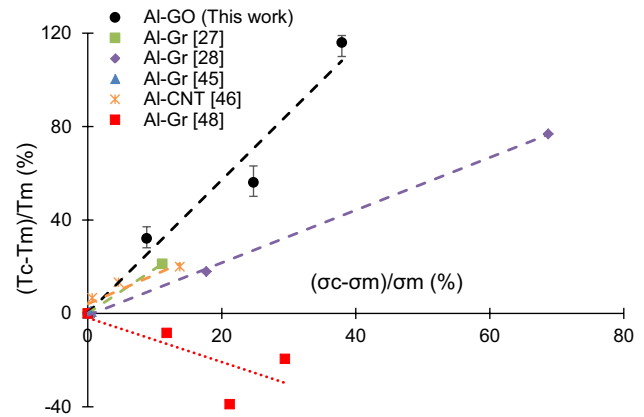


Fig. 14 Comparison of the strengthening and stiffening efficiencies of various reinforcements in Al matrix composites

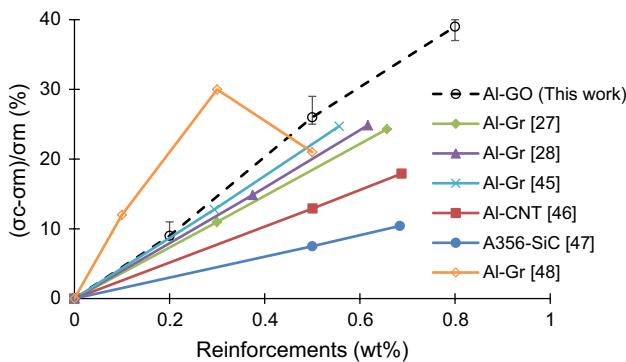


Fig. 13 Strengthening increment of various reinforcements in the Al matrix composites

stiffening efficiency with those of other Al matrix composites strengthened by other published reports.

As in Eq. (9), the stiffening efficiency (T), in a metal matrix composite is defined as the toughness increment:

$$T = 100 \times (T_c - T_m) / T_m \tag{10}$$

where T_c and T_m are the toughness of the composite and the matrix, respectively. According to Eqs. (9) and (10), It is indicated in Fig. 14 that the strengthening and stiffening efficiencies of GO in the Al-GO nanocomposites are higher than other researches. The key benefit of the GO strengthening is that form a strong interface and good bonding with the Al matrix, making it feasible for GO to much enforce its load bearing capability.

The efficiency of GO reinforcements against fracture depends on their distribution in the matrix, volume fraction, interfacial, wettability and their orientations. Magnesium particles were integrated to enhance the wettability between the Al matrix and GO particles. Therefore resulted in efficient load transfer from soft Aluminum matrix to strong GO nanoplates as obvious from strength and fracture strain of composites.

The mismatch in coefficient of thermal expansion (CTE), between Al ($CTE = 26 \times 10^{-6} K^{-1}$) and GO ($CTE = 1 \times 10^{-6} K^{-1}$) [49] may lead to the generation of dislocations at the interface. These dislocation results in increased strength of the composites. The Orowan looping is an impressive strengthening mechanism for reinforcement particles incorporated in a composite matrix [50]. The attendance of GO nanoplates in the Al matrix may lead to the formation of residual dislocation loops around reinforcement particle after a dislocation surrounded and bypass it. As a result, the produced loops may lead to high work hardening. Dispersion strengthening and load accommodation by the reinforcing particles are the major strengthening mechanisms reported in composites [51].

Based on the orowan theory, the shear stress (τ) required to move a moving dislocation among an array of impenetrable particles with the average spacing of λ can be written as follows [52]:

$$\tau = \frac{Gb}{\lambda} \tag{11}$$

where G is the shear modulus of matrix and b is the Burgers vector of moving dislocations. Equation (11) easily justifies the higher strength in the composites with more GO by considering the decrease in the spacing of the particles (λ). In addition to the dispersion strengthening of GO particles, the role they played in the matrix grain refinement should be also taken into account. As discussed earlier [Sect. 3.1, Eqs. (4)–(8)], the GO particles lead to the matrix grain refinement by increasing the rate of solidification and inhibiting the grain growth during hot rolling. It has been well documented that amongst the strengthening mechanisms only grain refining leads to a simultaneous increase in strength and ductility [53]. The improved strength in the fine-grained composites is due to the grain boundaries because they act as the barriers against the matrix dislocations. The relationship between strength and grain size is often described by the Hall–Petch equation as follows [51]:

$$\sigma_0 = \sigma_i + KD^{-0.5} \quad (12)$$

where σ_0 is the yield or tensile strength, σ_i is the lattice internal friction against dislocation movement, K is a constant and D refers to the average grain size. According to this, the improvement in the strength (S_y and S_{uts}) of fabricated composites, shown in Fig. 12 is associated with the contribution between progressive grain refinement and dispersion strengthening. Previous investigations have shown that the increase in strength of composites is often accompanied by decrease in ductility [27, 54, 55]. The loss of ductility is mostly attributed to the cracking between the interface of matrix and reinforcement. Therefore, the improved ductility of fabricated composites implies that the bond between the Al matrix and GO nanoplates is strong enough to withstand against premature interface cracking. In addition, the grain refining of the matrix by the GO particles (Fig. 5) enhances ductility and even covers the negative effect of the agglomeration of particles shown in Fig. 7c, d [56].

Figure 15 shows the SEM images of the fracture surface of the tensile specimens with two magnifications. All the micrographs are evidently typical of ductile fracture with pronounced dimples on the fracture surface. The dimples nucleate when the bond between particles or inclusions with the matrix is detached. Alternatively, stress concentration at the triple junctions of grain boundaries or at grain corners may cause the nucleation of dimples [57]. In ductile fractures, such as the behavior of fabricated composites, the dimple nucleation, the dimple growth, formation of micro-cracks by the coalescence of dimples and crack propagation take place sequentially before the final fracture. The size of dimples is an index to the ductility of material so that larger dimples are observed for more ductile materials. Unlike to the fracture surface of the base metal in Fig. 15a, those of fabricated composites in Fig. 15b–d are characterized by

a combination of large and small dimples. This characteristic easily leads one to conclude that the material is composed of constituents with different ductility characteristics. The local ductility in a composite depends on the grain size and the distribution of reinforcing particles. Indeed, the larger and deeper dimples are associated with the regions with higher ductility which is likely due to the Al matrix with fine-grained microstructure. It is evident that the area of regions with large dimples has increased with increase in the weight percent of GO. This is consistent with the microstructural observations in Fig. 5, confirming the modification of matrix grain size by the GO particles. These results are in good agreement with other reports in the literature about the fracture behavior of Mg and Al composites with graphene [50, 58].

There results of hardness testing are presented in Fig. 16. It is observed that the hardness of all nanocomposite specimens is higher than that of the base alloy. It is surprising that hardness increases by about 40% with the addition of 0.8 wt% of GO. This observation is in good agreement with the results of tensile testing in Fig. 12. As discussed, the effect of GO on increasing the hardness can be ascribed to a synergistic effect of matrix grain refinement, load bearing by the nanoparticle and the role of particles as barriers against the free motion of dislocations [59]. It seems that hardness keeps the increasing trend for further contents of GO due to the mentioned strengthening mechanisms.

4 Conclusions

In the present study, Al6061 nanocomposites reinforced with 0.2, 0.5 and 0.8 wt% of graphene oxide (GO) nanoplates were fabricated by stir casting and hot rolling processes. Microstructure and mechanical properties of the nanocomposites were investigated and predicted by micro-mechanical models. The novelty of this research is that we have been able to produce bulk nanocomposites with high strength and toughness, with the simultaneous use of the stir casting and hot rolling process. The followings are the major outcomes of this research:

- (1) Optical microscopy observations showed that adding GO leads to considerable grain refinement in the matrix. Also, the morphology of grains changed from columnar to equiaxed in the composites with increasing of GO. Working as nucleant in the molten Al and grain growth inhibitor during hot rolling were found as the dominant mechanisms through which the GO nanoplates could result in the grain refinement.
- (2) The SEM micrographs showed that the agglomeration of the particles increases in some areas. Although,

Fig. 15 SEM images from the fracture surfaces: **a** base metal (0 wt% GO) and Al6061-GO composites with **b** 0.2, **c** 0.5 and **d** 0.8 wt% GO, with two magnifications

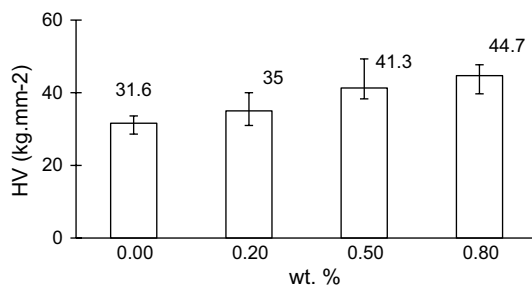
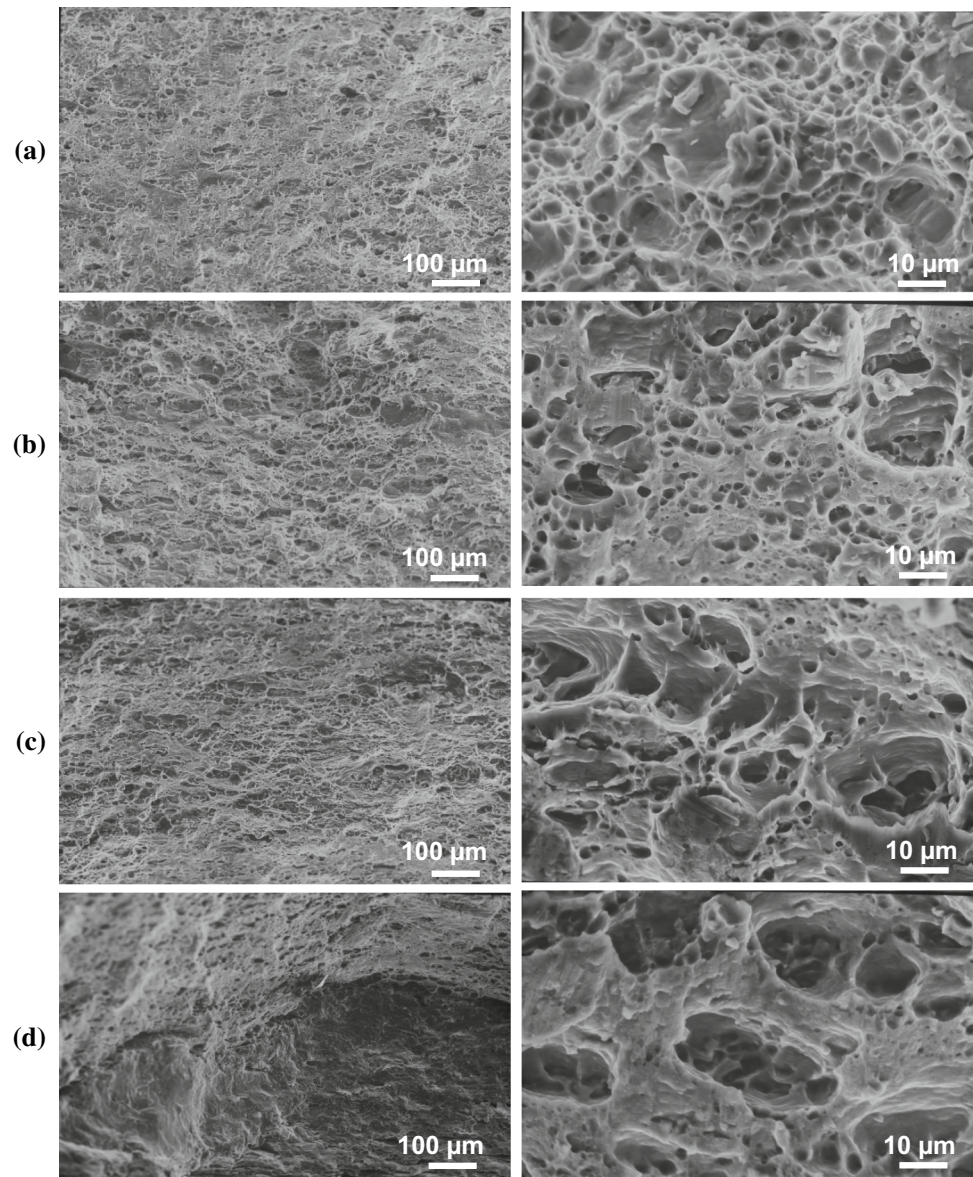


Fig. 16 Vickers hardness of Al-GO nanocomposite in terms of weight percentage of reinforcements

the grain refining of the matrix by the GO particles enhances the ductility and even covers the negative effect of the agglomeration of particles.

- (3) By using backscattered image and EDS map analysis of carbon, it is inferred that the GO particles have been uniformly distributed within the Al matrix.
- (4) It was confirmed that porosities increase with the increase in the content of GO. The release of confined air between particles during stir casting is the possible reason for the appearance of porosities at the vicinity of GO particles. Also on average, after performing the hot rolling process, the porosity value decreased by about 56% comparing with the casting state.
- (5) The tensile test results showed that the yield strength, ultimate strength, ductility and toughness increase with the increase in the content of GO up to 43, 38 and 58 and 116%, respectively. Also, the hardness of fabricated nanocomposites considerably increased (40% for 0.8 wt% GO composite). The accompanying increase in

the strength and ductility of fabricated nanocomposites was attributed to the remarkable grain refinement in the presence of GO. Graphene oxide nanoplates having a high specific surface area also avoid the movement of cracks in the nanocomposites, leading to a considerable increase in toughness.

- (6) The observation of fractured surfaces showed that ductile fracture has been the dominant mechanism for the studied composites. These results confirmed the improvement of toughness by adding GO nanoplates.

References

- M. Khademian, A. Alizadeh, A. Abdollahi, *Trans. Indian Inst. Met.* **70**, 1635 (2017)
- Y. Li, Y.H. Zhao, V. Ortalan, W. Liu, Z.H. Zhang, R.G. Vogt, N.D. Browning, E.J. Lavernia, J.M. Schoenung, *Mater. Sci. Eng. A* **527**, 305 (2009)
- J. Oñoro, M.D. Salvador, L.E.G. Cambronero, *Mater. Sci. Eng. A* **499**, 421 (2009)
- A. Yazdani, E. Salahinejad, *Mater. Des.* **32**, 3137 (2011)
- J.-H. Kim, J.-G. Jung, E.-J. Baek, Y.S. Choi, K. Euh, *Met. Mater. Int.* **25**, 353 (2019)
- B. Prabhu, C. Suryanarayana, L. An, R. Vaidyanathan, *Mater. Sci. Eng. A* **425**, 192 (2006)
- I. Ozdemir, S. Ahrens, S. Mücklich, B. Wielage, *J. Mater. Process. Technol.* **205**, 111 (2008)
- M. Alizadeh, M.H. Paydar, *J. Alloys Compd.* **492**, 231 (2010)
- A. Mazahery, M.O. Shabani, *Powder Technol.* **217**, 558 (2012)
- Z. Sadeghian, M.H. Enayati, P. Beiss, *J. Mater. Sci.* **44**, 2566 (2009)
- K. Sivaprasad, S.P.K. Babu, S. Natarajan, R. Narayanasamy, B.A. Kumar, G. Dinesh, *Mater. Sci. Eng. A* **498**, 495 (2008)
- M. Komarasamy, R.S. Mishra, J.A. Baumann, G. Grant, Y. Hovanski, *Friction Stir Welding and Processing VII* (Springer, Cham, 2013), pp. 39–46
- T. Varol, A. Canakci, *Philos. Mag. Lett.* **93**, 339 (2013)
- M.P. De Cicco, X. Li, L.-S. Turng, *J. Mater. Process. Technol.* **209**, 5881 (2009)
- H. Asgharzadeh, M. Sedigh, *J. Alloys Compd.* **728**, 47 (2017)
- X. Hu, X. Zhang, M. Tian, L. Qu, S. Zhu, G. Han, *J. Compos. Mater.* **50**, 2365 (2016)
- R.J. Young, I.A. Kinloch, L. Gong, K.S. Novoselov, *Compos. Sci. Technol.* **72**, 1459 (2012)
- H.G. Prashantha Kumar, M. Anthony Xavier, *Procedia Eng.* **97**, 1033 (2014)
- Z. Duan, L. Zhang, Z. Lin, D. Fan, M. Saafi, J. Castro Gomes, S. Yang, *J. Compos. Mater.* **52**, 3027 (2018)
- S.K. Thandalam, S. Ramanathan, S. Sundarrajan, *J. Mater. Res. Technol.* **4**, 333 (2015)
- L. He, Y. Liu, J. Li, B. Li, *Mater. Des.* (1980–2015) **36**, 88 (2012)
- S.B. Venkata Siva, K.L. Sahoo, R.I. Ganguly, R.R. Dash, S.K. Singh, B.K. Satpathy, G. Srinivasarao, *Metall. Mater. Trans. B* **44**, 800 (2013)
- R.N. Rai, A.K.P. Rao, G.L. Dutta, M. Chakraborty, *Mater. Sci. Forum* **765**, 418 (2013)
- H. Lee, J.H. Choi, M.C. Jo, I. Jo, S.-K. Lee, S. Lee, *Met. Mater. Int.* **24**, 894 (2018)
- J.H. Shin, H.J. Choi, D.H. Bae, *Mater. Sci. Eng. A* **578**, 80 (2013)
- A.M. El-Sabbagh, M. Soliman, M.A. Taha, H. Palkowski, *J. Mater. Process. Technol.* **213**, 1669 (2013)
- S. Yan, C. Yang, Q. Hong, J. Chen, D. Liu, S. Dai, *J. Mater. Eng.* **1**, 1 (2011)
- M. Rashad, F. Pan, A. Tang, M. Asif, *Prog. Nat. Sci. Mater. Int.* **24**, 101 (2014)
- C.-H. Jeon, Y.-H. Jeong, J.-J. Seo, H.N. Tien, S.-T. Hong, Y.-J. Yum, S.-H. Hur, K.-J. Lee, *Int. J. Precis. Eng. Manuf.* **15**, 1235 (2014)
- S.E. Shin, H.J. Choi, J.H. Shin, D.H. Bae, *Carbon* **82**, 143 (2015)
- W.S. Hummers, R.E. Offeman, *J. Am. Chem. Soc.* **80**, 1339 (1958)
- W. Li, W. Wu, Z. Li, *ACS Nano* **12**, 9309 (2018)
- C. Millière, M. Suéry, *Mater. Sci. Technol.* **4**, 41 (1988)
- R.K. Gupta, Z.A. Alahmed, F. Yakuphanoglu, *Mater. Lett.* **112**, 75 (2013)
- H.P. Myers, *Introductory Solid State Physics*, 2nd edn. (CRC Press, Boca Raton, 1997)
- Y. Sheng, X. Tang, E. Peng, J. Xue, *J. Mater. Chem. B* **1**, 512 (2013)
- M. Alipour, R. Eslami-Farsani, *Mater. Sci. Eng. A* **706**, 71 (2017)
- C.R. Manning, T.B. Gurganus, *J. Am. Ceram. Soc.* **52**, 115 (1969)
- P. Baumli, J. Sytchev, G. Kaptay, *J. Mater. Sci.* **45**, 5177 (2010)
- D. Wu, T.G. Nieh, *Mater. Sci. Eng. A* **609**, 110 (2014)
- D.A. Porter, K.E. Easterling, M.Y. Sherif, *Phase Transformations in Metals and Alloys*, 3rd edn. (CRC Press, New York, 2009)
- X. Gong, W. Gong, S.B. Kang, J.H. Cho, X. Gong, W. Gong, S.B. Kang, J.H. Cho, *Mater. Res.* **18**, 360 (2015)
- A. Sarkar, S. Sanyal, T.K. Bandyopadhyay, S. Mandal, *Mater. Sci. Eng. A* **703**, 205 (2017)
- D.D.L. Chung, *Carbon Composites: Composites with Carbon Fibers, Nanofibers, and Nanotubes*, 2nd edn. (Elsevier Science, Amsterdam, 2017)
- J.L. Li, Y.C. Xiong, X.D. Wang, S.J. Yan, C. Yang, W.W. He, J.Z. Chen, S.Q. Wang, X.Y. Zhang, S.L. Dai, *Mater. Sci. Eng. A* **626**, 400 (2015)
- J. Liao, I. Sridhar, *Mater. Des.* **31**, S96 (2010)
- Y. Yang, J. Lan, X. Li, *Mater. Sci. Eng. A* **380**, 378 (2004)
- X. Gao, H. Yue, E. Guo, H. Zhang, X. Lin, L. Yao, B. Wang, *Mater. Des.* **94**, 54 (2016)
- F.A. Mirza, D.L. Chen, *Nanosci. Nanotechnol. Lett.* **4**, 794 (2012)
- M. Rashad, F. Pan, H. Hu, M. Asif, S. Hussain, J. She, *Mater. Sci. Eng. A* **630**, 36 (2015)
- R.O. Scattergood, C.C. Koch, K.L. Murty, D. Brenner, *Mater. Sci. Eng. A* **493**, 3 (2008)
- G.E. Dieter, D.J. Bacon, *Mechanical Metallurgy* (McGraw-Hill, New York, 1986)
- H. Xu, Z. Lu, D. Wang, C. Liu, *Nucl. Eng. Technol.* **49**, 178 (2017)
- S.E. Shin, H.J. Choi, J.H. Shin, D.H. Bae, *Carbon* **82**, 143 (2015)
- M. Khatami, A. Fattah-alhosseini, Y. Mazaheri, M.K. Keshavarz, M. Haghshenas, *Int. J. Adv. Manuf. Technol.* **93**, 681 (2017)
- M. Rashad, F. Pan, A. Tang, M. Asif, S. Hussain, J. Gou, J. Mao, *J. Ind. Eng. Chem.* **23**, 243 (2015)
- A. Das, *Metall. Mater. Trans. A* **49**, 1425 (2018)
- M. Rashad, F. Pan, Z. Yu, M. Asif, H. Lin, R. Pan, *Prog. Nat. Sci. Mater. Int.* **25**, 460 (2015)
- A. El-Sabbagh, M. Soliman, M. Taha, H. Palkowski, *J. Mater. Process. Technol.* **212**, 497 (2012)

Publisher's Note Springer Nature remains neutral with regard to jurisdictional claims in published maps and institutional affiliations.